remote sensing

MDPI

Article

Retrieval and Validation of XCO_2 from TanSat Target Mode Observations in Beijing

Zhengyi Bao [1,2], Xingying Zhang [3,*], Tianxiang Yue [1,2], Lili Zhang [4], Zong Wang [1,2], Yimeng Jiao [1,2], Wenguang Bai [3] and Xiaoyang Meng [5]

1 State Key Laboratory of Resources and Environmental Information System, Institute of Geographical Sciences and Natural Resources Research, Chinese Academy of Sciences, Beijing 100101, China; bzy@lreis.ac.cn (Z.B.); yue@lreis.ac.cn (T.Y.); wangzong@lreis.ac.cn (Z.W.); jiaoym@lreis.ac.cn (Y.J.)
2 College of Resources and Environment, University of Chinese Academy of Sciences, Beijing 100049, China
3 National Satellite Meteorological Center, China Meteorological Administration, Beijing 100081, China; baiwg@cma.gov.cn
4 Aerospace Information Research Institute, Chinese Academy of Sciences, Beijing 100094, China; zhangll@lreis.ac.cn
5 Institute of Electrical Engineering, Chinese Academy of Sciences, Beijing 100190, China; mengxiaoyang@mail.iee.ac.cn
* Correspondence: zxy@cma.gov.cn

Received: 28 August 2020; Accepted: 17 September 2020; Published: 18 September 2020

Abstract: Satellite observation is one of the main methods used to monitor the global distribution and variation of atmospheric carbon dioxide (CO_2). Several CO_2 monitoring satellites have been successfully launched, including Japan's Greenhouse Gases Observing SATellite (GOSAT), the USA's Orbiting Carbon Observatory-2 (OCO-2), and China's Carbon Dioxide Observation Satellite Mission (TanSat). Satellite observation targeting the ground-based Fourier transform spectrometer (FTS) station is the most effective technique for validating satellite CO_2 measurement precision. In this study, the coincident observations from TanSat and ground-based FTS were performed numerous times in Beijing under a clear sky. The column-averaged dry-air mole fraction of carbon dioxide (XCO_2) obtained from TanSat was retrieved by the Department for Eco-Environmental Informatics (DEEI) of China's State Key Laboratory of Resources and Environmental Information System based on a full physical model. The comparison and validation of the TanSat target mode observations revealed that the average of the XCO_2 bias between TanSat retrievals and ground-based FTS measurements was 2.62 ppm, with a standard deviation (SD) of the mean difference of 1.41 ppm, which met the accuracy standard of 1% required by the mission tasks. With bias correction, the mean absolute error (MAE) improved to 1.11 ppm and the SD of the mean difference fell to 1.35 ppm. We compared simultaneous observations from GOSAT and OCO-2 Level 2 (L2) bias-corrected products within a ±1° latitude and longitude box centered at the ground-based FTS station in Beijing. The results indicated that measurements from GOSAT and OCO-2 were 1.8 ppm and 1.76 ppm higher than the FTS measurements on 20 June 2018, on which the daily observation bias of the TanSat XOC_2 results was 1.87 ppm. These validation efforts have proven that TanSat can measure XCO_2 effectively. In addition, the DEEI-retrieved XCO_2 results agreed well with measurements from GOSAT, OCO-2, and the Beijing ground-based FTS.

Keywords: TanSat; target mode; XCO_2 retrieval; validation; Beijing FTS

1. Introduction

Carbon dioxide (CO_2) is the dominant anthropogenic greenhouse gas in the atmosphere and plays an important role in global climate change [1]. Affected by human activities such as the burning

of fossil fuels and changes in land use, CO_2 concentration has risen sharply from 280 parts per million (ppm) in pre-industrial times to 410 ppm in 2018; the annual growth reached 3 ppm in 2015. Current knowledge regarding the temporal and spatial variability of CO_2 is however still limited by data uncertainty caused by observation conditions and model simulation capability [2, 3]. These limitations generate large gaps in our understanding of natural and anthropogenic surface carbon sources and sinks. In recent years, several CO_2 monitoring techniques have been developed to deal with these issues [4–6]. Large-scale observations of the column-averaged dry-air mole fraction of CO_2 (XCO_2) can now be obtained by satellite remote sensing.

XCO_2 can be retrieved from different types of spectral coverage, of which three near-infrared bands (the O_2 A-band at 0.76 μm and two CO_2 bands at 1.61 μm and 2.06 μm) are widely used due to their sensitivity to variations in surface CO_2. The global XCO_2 distribution was first obtained from the SCanning Imaging Absorption spectroMeter for Atmospheric CHartographY (SCIAMACHY) on board the European Environmental Satellite (Envisat) as satellite measurements [7] with a spectral detection range of 240–2380 nm, covering the O_2-A and CO_2 bands. Subsequently, CO_2 remote sensing satellites have been designed and launched with higher spectral and spatiotemporal resolutions.

China's global carbon dioxide observation satellite (TanSat), Japan's Greenhouse Gases Observing Satellite (GOSAT), and the USA's Orbiting Carbon Observatory-2 (OCO-2) are three representative CO_2 remote sensing satellites currently in orbit, which were launched in 2016, 2009, and 2014, respectively [8–10]. TanSat is China's first atmospheric CO_2 observation satellite [11–13] and carries the Atmospheric Carbon-dioxide Grating Spectroradiometer (ACGS) to measure the near-infrared absorption of CO_2, along with the Cloud and Aerosol Polarimetry Imager (CAPI) to compensate for CO_2 measurement errors by performing high-resolution cloud and aerosol measurements [14]. A comparison of TanSat, OCO-2, and GOSAT is provided in Table 1.

Table 1. Parameters of the Carbon Dioxide Observation Satellite (TanSat), Orbiting Carbon Observatory-2 (OCO-2), and Greenhouse Gases Observing SATellite (GOSAT).

Satellite	TanSat	OCO-2	GOSAT
Country	China	USA	Japan
Launch year	2016	2014	2009
Gas detected	O_2, CO_2	O_2, CO_2	CO_2, CH_4, O_2, O_3, H_2O
Onboard instruments	ACGS, CAPI	Three parallel high-resolution near-infrared spectrometers	TANSO-FTS, TANSO-CAI
Spectrometers	Grating	Grating	Interferometry
Spectrum for CO_2 (μm)	0.758–0.778 1.59–1.62 2.04–2.08	0.757–0.772 1.59–1.62 2.04–2.08	0.758–0.775 1.56–1.72 1.92–2.08
Swath (km)	20	10	790
Signal-to-noise ratio of CO_2 sounder	Band1: > 360 Band2: > 250 Band3: > 180	Band2: > 300 Band3: > 240	> 300
Observation mode	Nadir, glint, target	Nadir, glint, target	Nadir, glint, target
Orbit altitude (km)	705	705	666
Repeating period (days)	16	16	3

Spatial resolution for nadir mode (km)	2 × 2	1.29 × 2.25	10.5

Note: ACGS represents the Atmospheric Carbon-dioxide Grating Spectroradiometer; CAPI represents the Cloud and Aerosol Polarimetry Imager; TANSO-FTS represents the Thermal And Near infrared Sensor for carbon Observation–Fourier Transform Spectrometer; TANSO-CAI represents the Cloud and Aerosol Imager.

Many approaches have been devised for XCO_2 retrieval using different models [15–21]. The atmospheric radiative transfer model simulates the physical process of sunlight transmission through the atmosphere. XCO_2 can be retrieved by fitting the satellite measurements with the physical model simulation results. The most widely utilized inverse method is the optimal estimation method (OEM), which has been used to retrieve XCO_2 for Level 2 (L2) satellite products. In order to determine the accuracy of the retrieved XCO_2 and to correct the bias with the true values, space-based observations must be compared with measurements from other sources, including ground-based instruments [22].

Several research studies have been carried out to validate the accuracy of the XCO_2 retrieval algorithm with different satellites. Buchwitz et al. validated the SCIAMACHY data products retrieved using the weighting function modified differential optical absorption spectroscopy (WFM-DOAS) algorithm [23]. Reuter et al. validated the Bremen Optimal Estimation DOAS (BESD) algorithm retrieval of SCIAMACHY data based on Fourier transform spectrometer (FTS) measurements [24]. O'Dell et al. described and validated the Atmospheric CO_2 Observations from Space (ACOS) retrieval algorithm with GOSAT data [18]; and Oshchepkov et al. performed GOSAT data retrieval using the photon path-length probability density function (PPDF) algorithm validated by the Total Carbon Column Observing Network (TCCON) sites [25]. Yoshida et al. validated the official GOSAT product retrieved using the National Institute for Environmental Studies (NIES) algorithm using TCCON data [26]. Wunch et al. compared the OCO-2 official XCO_2 product from the ACOS algorithm with TCCON data, completing the first validation of the OCO-2 target mode that provided a bias correction for nadir mode and glint mode XCO_2 retrieval [27]. Bi et al. validated OCO-2 observations with the Beijing ground-based FTS site, which provided a reliable method for TanSat validation [28]. For TanSat, Liu et al. retrieved XCO_2 with the Institute of Atmospheric Physics, Chinese Academy of Sciences (IAPCAS) algorithm using nadir mode and validated the results with TCCON sites [29].

It is worth mentioning that the TanSat target mode has yet to be validated with ground-based measurements, which is needed to correct the bias of satellite observations. Herein, the Department for Eco-Environmental Informatics (DEEI) of the State Key Laboratory of Resources and Environmental Information System retrieved XCO_2 measured from TanSat by coupling the SCIATRAN model and the OEM method. For the first time, TanSat target mode observations were retrieved and validated with measurements from GOSAT, OCO-2, and the Beijing ground-based FTS site in this study.

2. Data

TanSat target mode data and ground-based FTS XCO_2 data are indispensable factors needed to perform validation. In this study, these data were provided by the National Satellite Meteorological Center (NSMC) of the China Meteorological Administration. The TanSat data consisted of calibrated and geolocated spectra information from space observations, and the format was the Hierarchical Data Format version 5 (HDF5) format, whereas the ground-based FTS data were the XCO_2 results measured and retrieved using the TCCON observation standards [28, 30].

2.1. Beijing Ground-Based FTS Measurement Data

The ground-based FTS observation station is located at 40.057°N, 116.275°E in Beijing, China and has been operated by the NSMC since 2015 [31]. The measurements were acquired using a Bruker 125HR FTS (Ettlingen, Germany), and the data collection was performed in accordance with the standards of TCCON. XCO_2 was retrieved using the GGG software package (GGG2014, Jet Propulsion Laboratory, Pasadena, California 91109, USA) provided by TCCON (https://tccon-

wiki.caltech.edu/GGG). The Beijing FTS was utilized to validate OCO-2, and the comparison method used in the previous study [28] provided a good approach for TanSat validation.

2.2. TanSat Target Mode Observation Data

In target mode observation, which is different from other observation modes, a point on the ground is scanned as the satellite passes overhead, an approach that is designed to obtain coincident data with ground-based measurements in order to correct the bias of XCO_2 measurements from the satellite. The Beijing ground-based FTS site has been observed as a target by TanSat several times since stable orbit was achieved. There were 10 days when TanSat scanned Beijing as a target in 2018, and the resulting observation data were then filtered for clouds and data quality, as shown in Table 2. TanSat data with an observation view angle > 50° were removed in order to reduce the uncertainty of the retrieved XCO_2. The observations of TanSat under cloudy conditions were filtered by cloud detection data from the FY-4A (http://satellite.nsmc.org.cn/), which is a new generation of China's geostationary meteorological satellites and provides cloud images every five minutes. The cloud flag product (CLM) used in this study was obtained from the Advanced Geostationary Radiation Imager (AGRI) on board the FY-4A. Figure 1 presents the view angle variation during TanSat target mode scanning, with the colors indicating measurement time. The insets in Figure 1. show the locations of the TanSat observation footprints and the ground-based FTS site in degrees latitude and longitude.

Table 2. Statistics of TanSat target mode observations with FY-4A cloud detection.

Observation date	Start time (UTC)	End time (UTC)	Observation view angle (°)		FY-4A cloud condition
			Minimum	Mean	
2018/03/08	04:50:48	04:54:42	38.4	43.24	Clear
2018/04/09	05:09:31	05:14:17	8.07	29.56	Clear
2018/04/16	05:19:47	05:24:31	9.79	30.15	Clear
2018/05/04	05:18:06	05:22:47	6.98	29.61	Clear
2018/05/24	05:05:14	05:09:45	16.04	31.17	Clear
2018/05/31	05:15:17	05:19:54	1.86	28.20	Clear
2018/06/20	05:02:12	05:06:45	20.91	34.22	Clear
2018/08/20	05:05:36	05:10:22	14.29	31.54	Clear
2018/11/21	05:24:39	05:29:27	18.68	33.22	Clear
2018/12/04	05:00:56	05:05:38	22.33	34.86	Clear

Note: UTC represents Coordinated Universal Time.

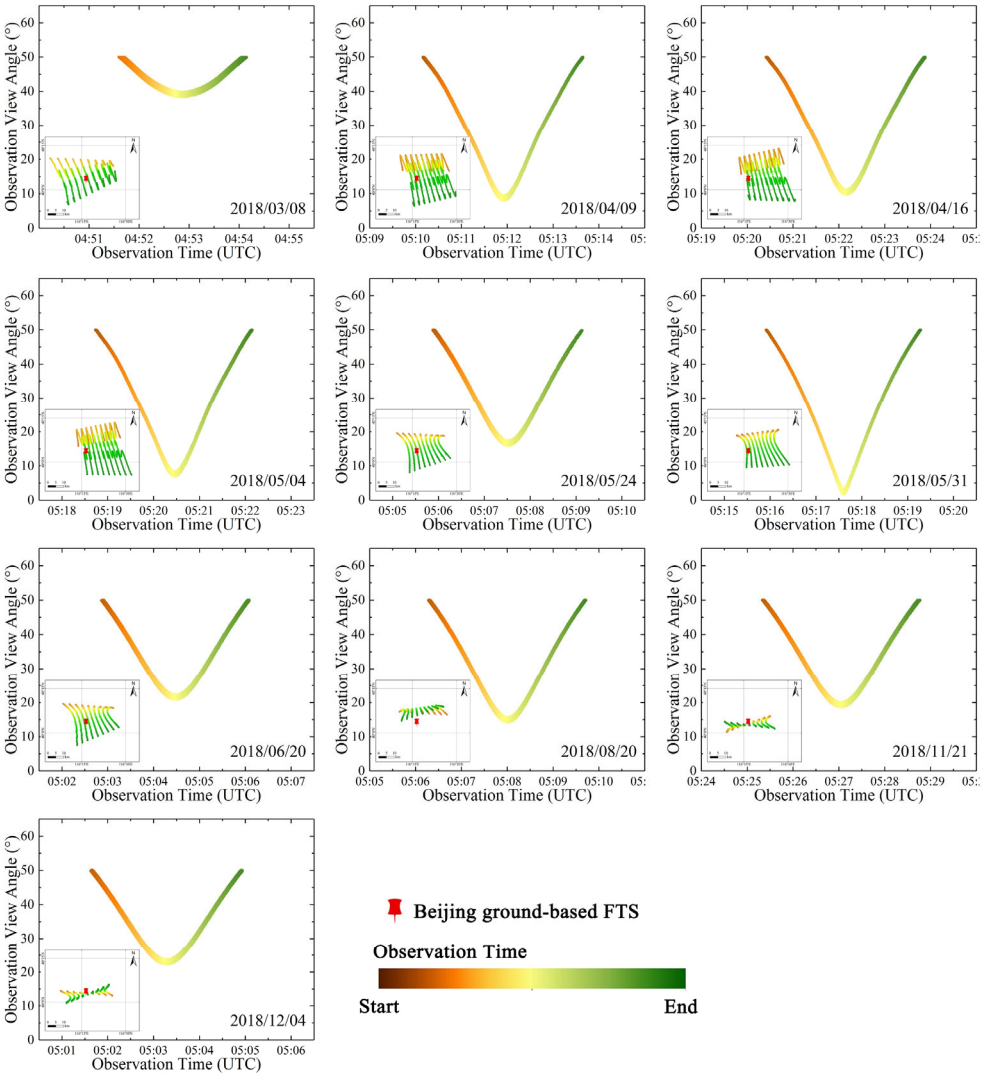

Figure 1. View angles and spatial distribution of TanSat target mode observations over Beijing in 2018. The *x*-axis is the observation time and the *y*-axis is the observation view angle. The left bottom inset in each panel depicts the locations of the Beijing Fourier transform spectrometer (FTS) site and TanSat footprints in degrees latitude and longitude. The red push pin represents the Beijing FTS site location. The colors indicate the measurement time in Coordinated Universal Time (UTC) of each observation.

3. Methods

In this study, the algorithm applied by the DEEI to retrieve XCO_2 from the TanSat observations was a full physical method based on the SCIATRAN [32] software package (SCIATRAN 3.1, Bremen, Germany) and the OEM [33]. As shown in Figure 2, SCIATRAN was the forward model, which was used to simulate the top of atmosphere (TOA) given a set of input parameters; OEM was the inverse method, which was used to solve the atmospheric CO_2 profile by fitting the simulated TOA spectrum with the instrument measurements. The major components of the DEEI algorithm, comprising the forward model, inverse method, input data, and XCO_2 calculation, are described below.

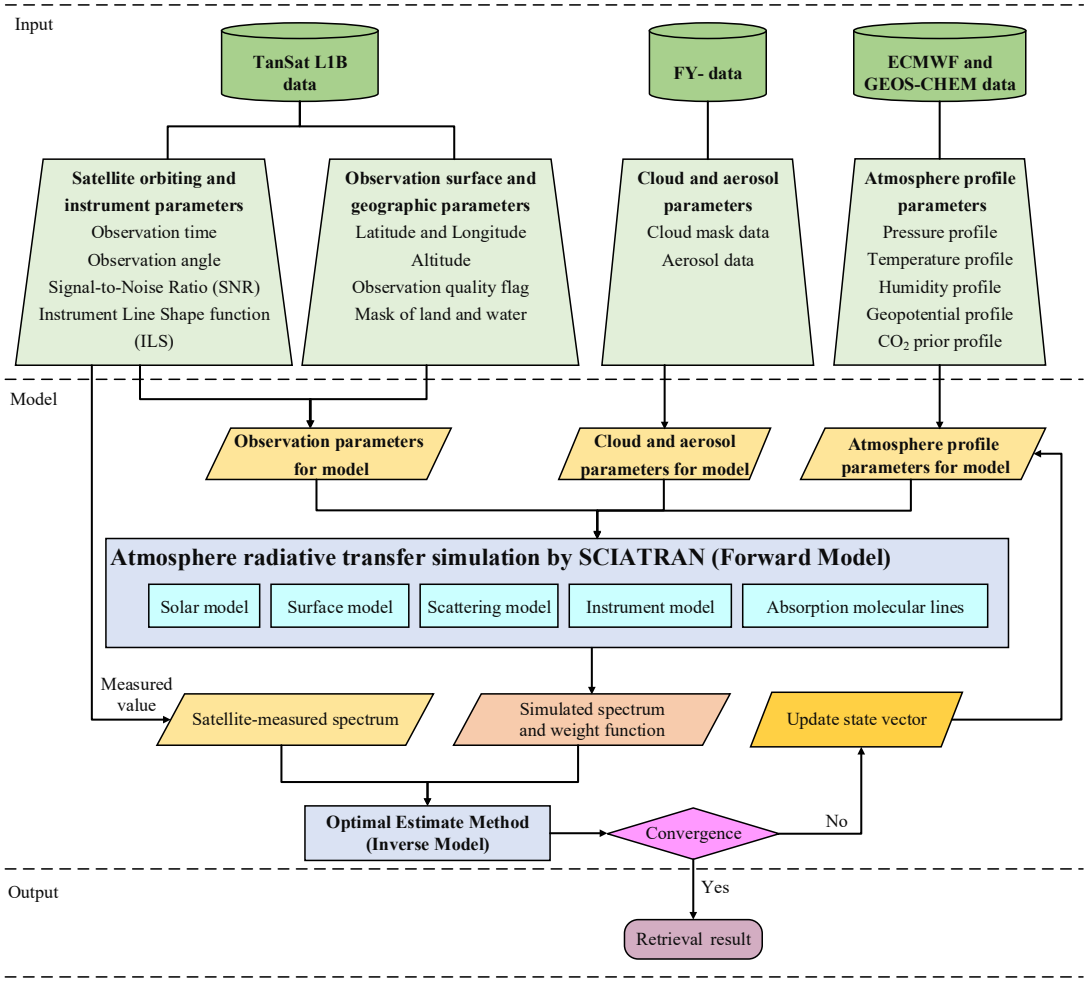

Figure 2. Flow chart of the Department for Eco-Environmental Informatics (DEEI) column-averaged dry-air mole fraction of carbon dioxide (XCO_2) retrieval algorithm.

3.1. Forward Model

The forward model is responsible for a numerical simulation of the satellite observation process. The input parameters needed by the simulation comprise the solar spectrum; atmospheric, physical, and chemical characteristics; surface features; and satellite instrument properties, with which the model can then complete the forward simulation of the observation process. The radiative transfer model is the core of the forward model and is designed to model the atmospheric radiative process; it simulates optical transmission, reflection, refraction, scattering, and radiation. Theoretically, the intensity of radiation observed by satellites from the TOA can be determined by these parameters and boundary conditions. Solving the radiative transfer equation is a very complex process, however, and is usually implemented through digital simulation using a radiative transfer model.

In this study, the forward simulation was performed based on the SCIATRAN model, which was developed by Bremen University to simulate the radiative transfer process within the ultraviolet–visible–infrared spectrum (175–4000 nm). The SCIATRAN model is capable of simulating spectral and angular distributions of the intensity or the Stokes vector of the transmitted, scattered, reflected, and emitted radiation by assuming either a plane-parallel or a spherical atmosphere [34, 35]. It is an open-source program and provides a very rich parameterized input interface. Users can modify and improve it to complete a wide variety of local tasks based on their own needs.

3.2. Inverse Method

The goal of satellite remote sensing is to analyze and calculate the physical and chemical properties of the atmosphere from the spectra observed by satellite instruments. The inversion process consists of searching a set of parameters in order to produce the "optimal" simulation of the observations. For atmospheric remote sensing retrieval, the iteration method is widely used to solve the inversion problem by minimizing the differences between the observed and synthetic spectra from each sounding. There are many methods used to perform the iteration process; of these, the Gauss–Newton and/or Levenberg–Marquardt (LM) algorithms are popular for remote sensing retrieval.

In this study, the inverse method used for retrieval was the Rodger's OEM [33]. Generally, the inversion problem can be conceptualized as building and solving a series of linear or nonlinear equations. The atmospheric state to be retrieved can be represented by the form of the following vector:

$$\mathrm{X} = (\mathrm{X}_1, \mathrm{X}_2, \ldots, \mathrm{X}_\mathrm{n}) \tag{1}$$

$$\mathrm{Y} = (\mathrm{Y}_1, \mathrm{Y}_2, \ldots, \mathrm{Y}_\mathrm{m}), \tag{2}$$

where X is the state vector to be retrieved, in which the subscript n represents the number of different atmospheric state parameters, and Y is the measurement vector, in which the subscript m represents the number of discrete measurements.

The radiance measured by satellites can be expressed as follows:

$$\mathrm{Y} = F(\mathrm{X}, b) + \varepsilon, \tag{3}$$

where F is the forward model describing the atmospheric radiative transfer process of the measurement; b is the set of parameters needed by the forward model, such as the profiles of temperature, humidity, pressure, surface albedo, and instrument line shape (ILS); and ε is the measurement noise and error from observation and simulation.

The cost function represents the cost generated by the iterations, which is defined as the difference between the forward model simulation and satellite observations. The optimal estimation can be obtained by minimizing the cost function in the following form:

$$J(x) = [y - F(x,b)]^T {S_\varepsilon}^{-1} [y - F(x,b)] + (x - x_a)^T {S_{ae}}^{-1} (x - x_a), \tag{4}$$

where S_ε is the error covariance matrix corresponding to the measurement vector, x_a is the vector of the prior state, and S_{ae} is the prior error variance matrix.

To solve the iteration problem, the LM method was selected in this study, as expressed by the following equation [36]:

$$x_{i+1} = x_i + \tilde{S}\left[K_i^T S_\varepsilon^{-1}\left(y - F(x_i - b)\right) - S_{ae}^{-1}(x_i - x_a)\right] \tag{5}$$

$$\tilde{S} = (K_i^T S_\varepsilon^{-1} K_i + (1+\gamma) S_{ae}^{-1})^{-1}, \tag{6}$$

where x_{i+1} and x_i represent the state vector at the iterations of $i+1$ and i, K_i is the weighting function matrix at iteration i, $\tilde{S}$ is the corresponding covariance matrix consisting of the variances of the retrieval state vector elements and their correlations, and γ is the damping factor.

3.3. XCO_2 Calculation Process for the DEEI Method

3.3.1. Information Extraction from TanSat L1B

TanSat L1B v2.0 data were used to retrieve the XCO_2 values in this study. Satellite observation information such as soundingID, latitude, longitude, height, angles, signal-to-noise ratio, and data quality flags can be extracted directly from TanSat L1B data based on the corresponding fields. In addition, the other TanSat L1B parameters needed by the retrievals are detailed below.

a) Polarization conversion processing

TanSat measures one direction of polarized light instead of the total intensity, whereas the simulation in the forward model is the Stokes vector I {*I, Q, U, V*}. Therefore, the simulated spectrum that is computed from the forward model needs to be converted into measurements using Stokes coefficients. The radiance measured from the TanSat ACGS can be expressed as follows [29]:

$$I_{ACGS} = I + \cos(2\theta) \cdot Q + \sin(2\theta) \cdot U, \quad (7)$$

where I, Q, and U represent the first three Stokes parameters; θ is the polarization angle, defined as the angle between the local meridian plane and the principal plane; and I_{ACGS} is the polarization-converted radiance measured by the ACGS.

b) ILS parameter information

TanSat measures the radiation spectra emitted from the top of the atmosphere. The measurement results are modulated by the linear function of the instrument. In the forward model, an ILS function is needed to convolve the simulated spectrum. For details regarding the radiometric calibration of TanSat, please refer to [37,38]. For XCO_2 retrieval, the ILS information for each footprint can be obtained individually from the corresponding fields of the TanSat L1B data.

3.3.2. Input Data and Databases

As depicted in Figure 2, a series of data and databases drives the radiative transfer model to simulate the process through the atmosphere. In addition to observational information from satellites, cloud condition and atmospheric profile data, the solar spectrum database, and the molecular atmospheric absorption lines are indispensable to the XCO_2 retrieval algorithm. The cloud detection data were from the coincident FY-4A CLM product and were used to filter the processable observation data, while the aerosol data were set as the model default parameters from the LOWTRAN database of SCIATRAN (http://www.iup.uni-bremen.de/sciatran/). The Kurucz solar irradiance database (http://kurucz.harvard.edu/sun/irradiance2008/) was selected as the solar spectrum data input. HITRAN 2012 has proven to be more accurate than its earlier version and was thus selected as the absorption database for the molecular spectral lines. For the atmospheric profiles, the temperature, humidity, surface pressure, and geopotential information were extracted from the ERA5-Interim database of the European Centre for Medium-Range Weather Forecasts (ECMWF) profiles (http://apps.ecmwf.int/datasets/). The database of atmospheric trace gas profiles was obtained from the Bremen 2D (B2D) chemical transport model, although the CO_2 profile was modified using the GEOS-Chem (http://acmg.seas.harvard.edu/geos/) simulation result as a prior value. Based on values from the prior CO_2 profile, a prior covariance matrix S_a was generated using Equation (8). The measurement covariance matrix could also be generated from the measurement values using Equation (8) as follows:

$$S_a(i,j) = \sigma^2 exp\left[-\frac{|Z_i - Z_j|}{r_c}\right], \quad (8)$$

where Z_i and Z_j are the height values corresponding to the elements i and j of the prior covariance matrix S_a, respectively, σ is the relative deviation, σ^2 is the diagonal element of S_a, and r_c is the correlation radius (km). In this study, σ^2 and r_c were set as 0.01% and 10 km, respectively.

3.3.3. XCO_2 Calculation from Retrieval Results

Based on the collocated satellite data and the databases described in Sections 3.3.1. and 3.3.2., the total amounts of the CO_2 and O_2 columns could be retrieved simultaneously using the weak CO_2 and O_2-A bands (1.61 μm and 0.76 μm) with SCIATRAN. In this study, XCO_2 was obtained by normalizing the CO_2 column with the O_2 column. Since the O_2 molecular changes in air are very small, O_2 is widely recognized as a gas that can accurately calculate the content of the air column. XCO_2 was then calculated as follows [39]:

$$X_{CO2} = \frac{CO_2^{col}}{O_2^{col}/O_2^{mf}}, \quad (9)$$

where CO_2^{col} and O_2^{col} are the retrieved absolute values of the CO_2 column and O_2 column, respectively (in molecules/cm^2); O_2^{mf} is the mole fraction of O_2 (assumed value, 0.2095); and O_2^{col}/O_2^{mf} converts the O_2 column into a corresponding dry air column.

4. Results and Comparison

As the first retrieval of the TanSat target mode observations by the DEEI, the XCO_2 results were validated with measurements from the Beijing ground-based FTS station. Furthermore, a preliminary bias correction was performed based on TanSat footprints, observation parameters, and ground-based FTS measurements. In addition, the near-simultaneous GOSAT and OCO-2 XCO_2 products were filtered for comparison with the TanSat bias-corrected XCO_2 results.

4.1. XCO_2 Retrieval Results

In 2018, TanSat orbited in target mode several times over Beijing, making observations on 8 March; 9 and 16 April; 4, 24, and 31 May; 20 June; 20 August; 21 November; and 4 December. XCO_2 was retrieved on each of these days, all of which had clear sky conditions. The data with the observation view angle > 50° were removed before retrieving. For the retrievals in each observation, the soundings where the differences between the XCO_2 values and mean values were higher than three times the standard deviation (SD) values were also removed as abnormal values. As shown by the retrieval result statistics in Table 3, most of the sounding numbers of the single-day observations were > 6000. The average XCO_2 value was 413.78 ppm in April, but by August it had decreased to 403.98 ppm, matching the XCO_2 seasonal variations in the Northern Hemisphere. The relatively large SD statistical values of 1.03 ppm and 1.19 ppm occurred in the measurements on 9 April and 24 May, respectively, while the minimum value of 0.17 ppm was found on 31 May. The mean value of 10 days' XCO_2 retrievals was 0.48 ppm, which met the high precision requirements of measurements and data quality filtering.

Table 3. TanSat XCO_2 statistics of target mode observation retrieval results.

Observation date	Sounding number	Minimum (ppm)	Maximum (ppm)	Mean (ppm)	SD (ppm)
2018/03/08	4449	409.52	411.79	411.31	0.43
2018/04/09	6304	410.24	417.27	413.78	1.03
2018/04/16	6303	410.19	412.54	411.76	0.51
2018/05/04	6052	409.95	411	410.49	0.25
2018/05/24	5377	409.54	414.33	412.03	1.19
2018/05/31	6141	409.74	410.59	410.19	0.17
2018/06/20	5865	406.64	408.48	407.2	0.33
2018/08/20	6269	402.05	404.54	403.98	0.29
2018/11/21	6053	410.31	411.5	410.92	0.27
2018/12/04	6028	411.2	413.33	412.87	0.3

Note: SD represents the standard deviation.

The XCO_2 SD statistics retrieved from each footprint are shown in Figure 3, from which the footprints' differences can be defined. The SD values of footprints 1–9 are close to the total SD values in coincident measurements, proving that the high SD values were not due to the measurement error of one footprint. The SD values > 1 ppm could have resulted from optical path misestimates caused by different view angles and aerosol optical depths. The preliminary retrieval statistics from the ACGS measurements proved that TanSat was orbiting stably and each footprint measured XCO_2 with high-quality precision.

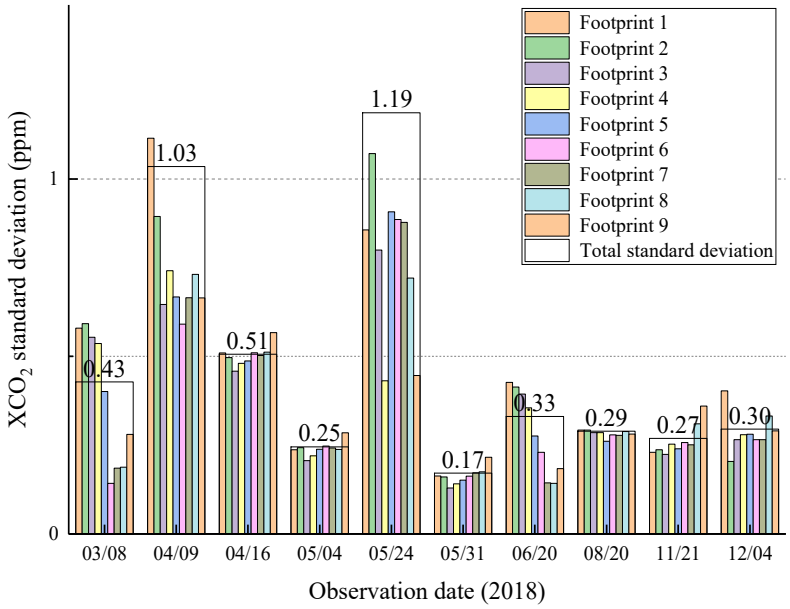

Figure 3. XCO_2 standard deviation (SD) statistics for the different footprints of each TanSat target mode measurement. The bars are color-coded to represent the SD values for the individual footprint of each day, and the numbers are the total statistical SD values for each single-day observation.

4.2. Validation against Beijing Ground-Based FTS Measurements

The Beijing FTS station is the point on the ground used in the TanSat target mode scanning, and provides the coincident ground-based measurement data. Different from the comparison with space-based observations, the validation of target mode observations against the ground-based FTS measurements has a large data volume capacity for spatiotemporal matching. In addition, the ground-based FTS in Beijing has been utilized to validate OCO-2 observations in previous studies [28], indicating the stable operation of the Beijing FTS measurements. In order to obtain rigorous matching results for validation, the ground-based FTS matching rule was set as ±0.5 h. As for TanSat, it only takes five minutes to pass the target observation area. As shown in Figure 4, all of the filtered TanSat soundings for XCO_2 retrieval were in the black rectangle near the Beijing ground-based FTS station. There were nine footprints around the Beijing FTS station, as depicted by the different colors in Figure 4a. The TanSat swung towards the target on the ground in order to take measurements during the target mode observations, causing the footprints to be curves, as opposed to straight lines.

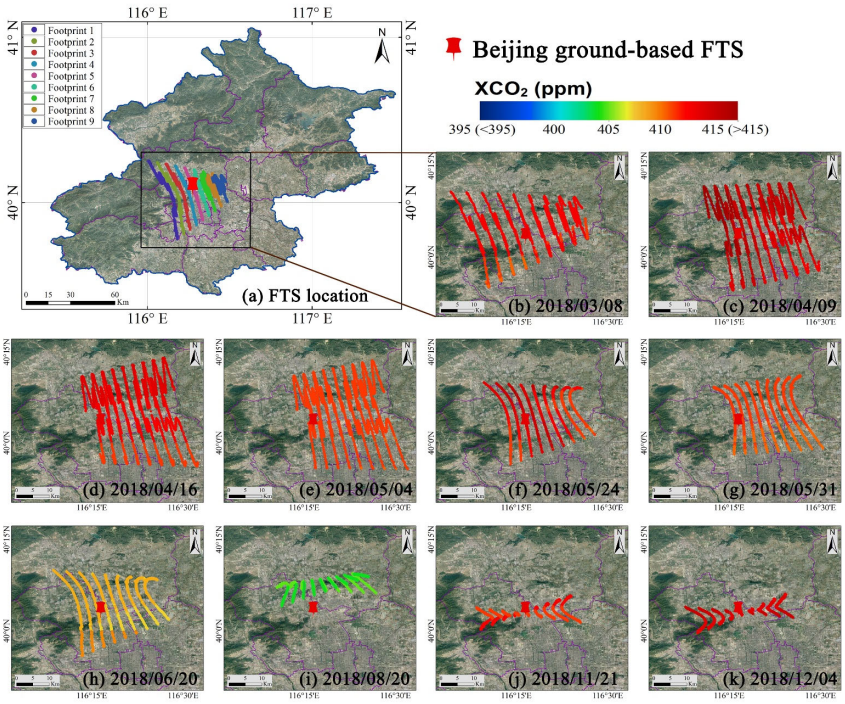

Figure 4. XCO_2 spatial distribution of TanSat target mode observations: (**a**) FTS location in Beijing and the nine footprints of the TanSat measurements; (**b–k**) XCO_2 spatial distribution retrieved from each target mode observation. The color bar in the upper right corner is the XCO_2 legend; the range from blue to red represents different XCO_2 values from low to high. The red push pin represents the Beijing FTS site.

The selected statistical data results for validation and bias analysis are listed in Table 4. A comparison of the space-based XCO_2 with the ground-based XCO_2 measurements for Beijing in 2018 revealed that the maximum XCO_2 measurement bias between TanSat and the FTS ground station occurred on 4 December, when it reached 4.85 ppm, while the minimum bias of 0.31 ppm occurred on 4 May. The total SD values in the last row of Table 4 were calculated by averaging the SD values for each day. The total SD values of the TanSat retrieval results and FTS measurements were 0.48 ppm and 0.29 ppm, respectively. The XCO_2 mean absolute error (MAE) between TanSat and the ground-based FTS was 2.62 ppm, and the SD of the mean difference in XCO_2 between TanSat and the ground-based FTS was 1.41 ppm. The comparison results indicated that the TanSat XCO_2 retrievals satisfied the requirement that the error be limited to 4 ppm (1%).

Table 4. XCO_2 (ppm) comparison between TanSat retrievals and ground-based FTS measurements.

Observation date	TanSat retrievals		FTS measurements		Bias
	Mean	SD	Mean	SD	
2018/03/08	411.31	0.43	408.43	0.25	2.88
2018/04/09	413.78	1.03	412.30	0.52	1.48
2018/04/16	411.76	0.51	410.57	0.29	1.19
2018/05/04	410.49	0.25	410.18	0.48	0.31
2018/05/24	412.03	1.19	408.06	0.32	3.97
2018/05/31	410.19	0.17	407.12	0.35	3.07
2018/06/20	407.2	0.33	403.30	0.11	3.9
2018/08/20	403.98	0.29	402.15	0.13	1.83
2018/11/21	410.92	0.27	408.24	0.17	2.68

2018/12/04	412.87	0.3	408.02	0.26	4.85
Total	-	0.48	-	0.29	2.62

4.3. Bias Correction

The comparison between the XCO_2 measurements from TanSat and the ground-based FTS measurements revealed that systematic biases arose in the XCO_2 retrievals. Bias correction is an indispensable procedure in data processing for GOSAT and OCO-2 [27, 40–42]. Generally, this consists of three main steps—parametric, footprint-level, and scaling bias correction. In this study, the bias correction was based on Equation (10). Parametric biases are functionally related to a given parameter associated with a given sounding; examples of this could be surface pressure, airmass, or retrieved aerosol quantities. In the DEEI method, since the surface pressure and aerosol parameters were not retrieved, the airmass factor was selected for parametric bias correction in this step. Footprint-level bias correction is to ensure that the same XCO_2 value of each footprint is obtained when observing similar scenes. Here, TanSat XCO_2 data were selected for analysis when all nine footprints converged in one sounding frame. The median XCO_2 was computed as the "true" value, and was subtracted from the observed XCO_2 in order to calculate the bias for each footprint. After the parametric and footprint-level bias corrections, the scaling bias was corrected in order to remove any global mean bias. The scaling coefficient was calculated by linear regression between the XCO_2 from TanSat and that from the ground-based FTS, with the intercept forced to zero, as follows:

$$X_{CO_2}^{corrected} = \frac{X_{CO_2}^{retrieved} - C_1(airmass - \overline{airmass}) - Bias_{footprint}(i)}{C_0}, \quad (10)$$

where $X_{CO_2}^{retrieved}$ represents the TanSat XCO_2 retrievals and $X_{CO_2}^{corrected}$ denotes the corrected XCO_2 data. $Bias_{footprint}(i)$ is the footprint bias for footprints i = 1…9; the adopted footprint biases for footprints 1–9 are 0.21, 0.26, 0.20, 0.10, 0.04, -0.03, -0.08, -0.15, and -0.06 ppm, respectively. C_0 is the scaling coefficient of TanSat and the ground-based FTS (calculated value, 1.0064), C_1 is the regression coefficient for the airmass (2.00 ppm/air mass was used in this study), and the overbar denotes the averages of all retrievals used for the regression analysis. Airmass is a simple function of the solar zenith angle θ_Z and the satellite viewing angle θ_V, and can be approximated as Equation (11) [40]:

$$airmass = \frac{1}{\cos\theta_Z} + \frac{1}{\cos\theta_V}, \quad (11)$$

The XCO_2 statistics for each step are listed in Table 5. As shown in Table 5, the bias of XCO_2 between TanSat and the ground-based FTS was improved by each step of the bias correction. The MAE of XCO_2 improved from 2.62 ppm to 2.60 ppm, 2.55 ppm, and 1.11 ppm following the step 1, step 2, and step 3 corrections, respectively. In addition, the SD of the mean difference in XCO_2 between TanSat and the ground-based FTS maintained the same value of 1.35 ppm in each step, which was 0.06 ppm lower than the 1.41 ppm value before correction. Figure 5 shows the comparison between the XCO_2 retrieved by TanSat and that retrieved by the ground-based FTS. As shown in Figure 5, the systematic errors in the TanSat retrieval results were present before bias correction (left panel), and decreased noticeably after bias correction (right panel).

Table 5. TanSat XCO_2 (ppm) statistics for the bias correction procedure.

Observation Date	**Step 1: Airmass Bias-Corrected Result**		**Step 2: Footprint Bias-Corrected Result**		**Step 3: Scaling Bias-Corrected Result**	
	Mean	**Bias**	**Mean**	**Bias**	**Mean**	**Bias**
2018/03/08	410.92	2.49	410.87	2.44	408.25	-0.18
2018/04/09	414.16	1.87	414.11	1.81	411.48	-0.82

2018/04/16	412.17	1.60	412.11	1.54	409.49	-1.08
2018/05/04	411.03	0.85	410.97	0.79	408.36	-1.82
2018/05/24	412.67	4.61	412.62	4.55	409.99	1.93
2018/05/31	410.85	3.73	410.80	3.68	408.19	1.06
2018/06/20	407.82	4.52	407.77	4.46	405.17	1.87
2018/08/20	404.47	2.31	404.41	2.26	401.84	-0.31
2018/11/21	409.23	1.00	409.18	0.94	406.58	-1.66
2018/12/04	411.08	3.06	411.02	3.00	408.41	0.39
MAE	-	2.60	-	2.55	-	1.11

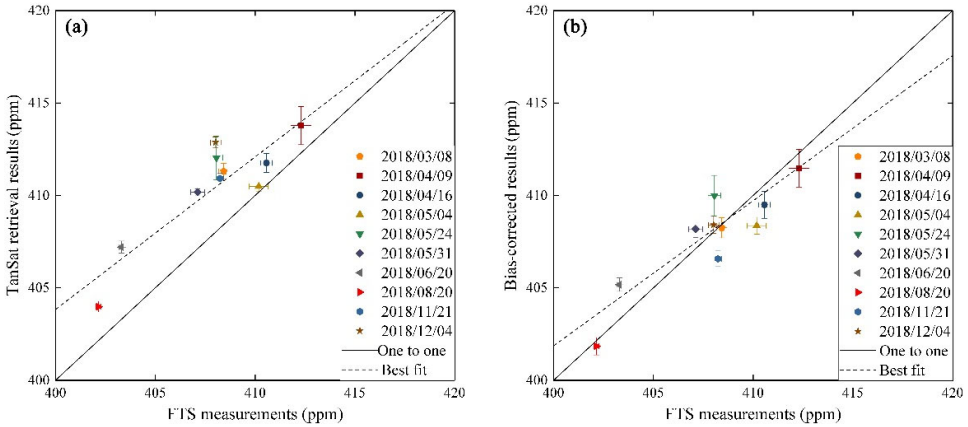

Figure 5. Comparison of XCO_2 retrieved from TanSat in target observation mode with the Beijing ground-based FTS measurements. The XCO_2 values of each observation date are represented by different shapes and colors; the error bars show the 1σ precision of the TanSat XCO_2 retrievals and the ground-based FTS measurements. The one-to-one line is solid, and the best fit line is dashed.

4.4. Comparison with Other XCO_2 Products

To date, the official TanSat L2 products have yet to be published. The Institute of Atmospheric Physics, Chinese Academy of Sciences (IAP-CAS) retrieved XCO_2 in the first half of 2017 from TanSat nadir mode observations and validated these measurements against those of the TCCON sites, finding an average bias of 2.11 ppm. In addition, the MAE of the DEEI-retrieved XCO_2 from the TanSat target mode observations was 2.62 ppm, which was 0.49 ppm higher than the IAP-CAS validation results. However, the XCO_2 MAE improved 1.11 ppm after bias correction, i.e., approximately half the average bias from the IAP-CAS.

As for the other CO_2 remote sensing satellites, GOSAT and OCO-2 were in orbit before TanSat was launched. Numerous types of products for XCO_2 have been created for GOSAT and OCO-2. In order to compare XCO_2 measured by TanSat with near-simultaneous observations from GOSAT and OCO-2, spatial matching was necessary. Regarding the GOSAT XCO_2 data, the SWIR L2 V02.81 product (https://data2.gosat.nies.go.jp/), which provides optimal XCO_2 retrieval results using fewer observation points, was employed for comparison in this study. For the OCO-2 XCO_2 data, the L2 V9r bias-corrected product (http://disc.sci.gsfc.nasa.gov/OCO-2) was selected for comparison with TanSat. In this study, all of the GOSAT and OCO-2 products were filtered with quality attributes prior to matching in order to obtain optimal measurements from space-based observations.

In terms of the comparison criteria, the matching method used in this study was the same as that used in previous studies [28]. Using the matching criteria of spatial and temporal separations within ±1° and ±2 h, respectively, some near-simultaneous XCO_2 data observed by GOSAT and OCO-2 were selected for comparison. Figure 6 presents the spatial distributions of the GOSAT and OCO-2 footprints. Due to the different footprint geolocations of the satellites, there was only a single-day observation of XCO_2 data on 20 June that matched the criteria for GOSAT and OCO-2. The data within the red square were selected for comparison. Table 6 lists the statistics of the comparison results for

the GOSAT, OCO-2, and TanSat measurements. The TanSat had more than 5000 soundings for comparison since it observed in target mode, and the lower standard deviation of the measurements was due to the retrieval-based data filtering and bias correction. For GOSAT and OCO-2, the total numbers of matched soundings were 15 and 187, respectively, and the corresponding mean values of XCO_2 were 405.10 ppm and 405.06 ppm. The biases of the comparison results between GOSAT, OCO-2, and TanSat and the Beijing ground-based FTS were 1.8 ppm, 1.76 ppm, and 1.87 ppm, respectively, indicating that the accuracy of the TanSat DEEI-retrieved and bias-corrected XCO_2 data was consistent with the accuracy of the GOSAT and OCO-2 L2 products, i.e., within a range of 1%.

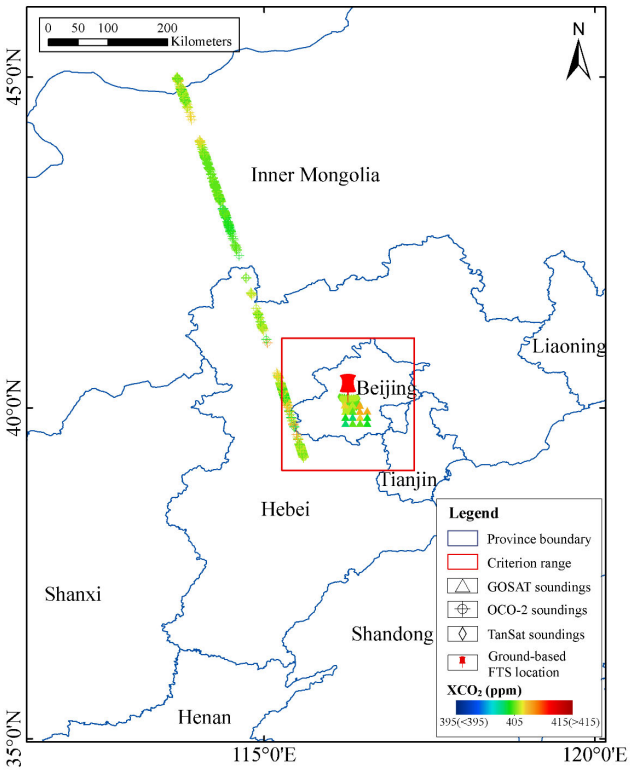

Figure 6. Spatial distribution of matched GOSAT, OCO-2, and TanSat soundings around the Beijing FTS site. Push pin: Beijing FTS site position; triangles: GOSAT soundings; hollow points with crosses: OCO-2 soundings; diamonds: TanSat soundings. The color range from blue to red represents different XCO_2 values from low to high; red rectangle: criterion range of ±1° latitude and longitude and ±2 h measuring time.

Table 6. Comparison of XCO_2 from TanSat with GOSAT and OCO-2 products.

Data statistic	GOSAT L2 products	OCO-2 L2 products	TanSat XCO_2 (bias-corrected)
Matched sounding number	15	187	5866
XCO_2 min (ppm)	402.35	401.19	404.19
XCO_2 max (ppm)	407.85	408.77	406.20
XCO2 mean (ppm)	405.10	405.06	405.17
SD (ppm)	1.63	1.09	0.36
Mean bias (ppm)	1.8	1.76	1.87

5. Conclusions and Outlook

This study performed the first validation of XCO_2 from the TanSat target mode observations retrieved by the DEEI algorithm using measurements from the Beijing FTS site. The retrieval results revealed that each instrument on board TanSat obtained XCO_2 measurements that did not exhibit any indication of abnormalities and had an SD range of 0.17–1.19 ppm. For the ground observation validation, the measured biases of the uncorrected retrievals ranged from 0.31 to 4.85 ppm, with an MAE of 2.62 ppm. Using preliminary bias correction, the TanSat XCO_2 MAE improved to 1.11 ppm, and the SD value of the mean difference between TanSat and ground-based FTS measurements improved to 1.35 ppm, from an initial value of 1.41 ppm. For other satellites, the comparison results showed that the simultaneous XCO_2 observations from GOSAT, OCO-2, and TanSat were 1.8 ppm, 1.76 ppm, 1.87 ppm higher than ground-based FTS measurements on 20 June 2018, respectively, proving that TanSat measurements were consistent with those of the GOSAT and OCO-2 products.

In future research, the DEEI algorithm will be improved with additional retrieval parameters. The satellite observation angle, surface attributes, and atmospheric parameters led to varying amounts of uncertainty, which should also be rectified in order to correct the retrieval results. Furthermore, since the retrieved data were filtered in order to retain only data collected under clear sky conditions and shallow aerosol optimal depths, aerosol rectification remains an important issue on which to focus.

Author Contributions: Conceptualization, Xingying Zhang, Tianxiang Yue, and Zhengyi Bao; data curation, Zhengyi Bao, Wenguang Bai, and Xiaoyang Meng; methodology, Xingying Zhang and Tianxiang Yue; software, Tianxiang Yue, Lili Zhang, and Zhengyi Bao; visualization, Zhengyi Bao, Zong Wang, and Yimeng Jiao; writing—original draft preparation, Zhengyi Bao; writing—review and editing, Zhengyi Bao, Xingying Zhang, and Tianxiang Yue. All authors have read and agreed to the published version of this manuscript.

Funding: This work was supported by the National Natural Science Funds of China (Grant Nos. 41590844, 41775028, 41421001, and 41930647), the Strategic Priority Research Program (A) of the Chinese Academy of Sciences (Grant No. XDA20030203), the National Key R&D Program of China (Grant Nos. 2017YFB0504001 and 2016YFB0500705), and the Innovation Project of LREIS (Grant No. O88RA600YA).

Acknowledgments: We are grateful to the members of the TanSat Science Team for the satellite data and ground-based FTS data used in this study. We are grateful to the NSMC of China for providing FY series products, the ECMWF for providing the meteorological data, the University of Bremen, Bremen, Germany, for providing the SCIATRAN model and B2D model, the GEOS-Chem Support Team for providing the GEOS-Chem software, the Harvard-Smithsonian Center for Astrophysics, Cambridge, MA 02138-2901, USA, for providing the HITRAN 2012 database, and Robert L. Kurucz for providing the online solar irradiance database. We thank the GOSAT Science Team and the OCO-2 Science Team for providing satellite products used in this study. We thank the TCCON Science Team for providing the data processing standards and software package. We thank Accdon (www.accdon.com) for its linguistic assistance during the preparation of this manuscript.

Conflicts of Interest: The authors declare no conflict of interest.

References

1. Intergovernmental Panel on Climate Change (IPCC). *Climate Change 2013: The Physical Science Basis. Contribution of Working Group I to the Fifth Assessment Report of the Intergovernmental Panel on Climate Change*; Cambridge University Press: Cambridge, UK; New York, NY, USA, 2013; p. 1535, doi:10.1017/CBO9781107415324.
2. Houweling, S.; Hartmann, W.; Aben, I.; Schrijver, H.; Skidmore, J.; Roelofs, G.J.; Breon, F.M. Evidence of systematic errors in SCIAMACHY-observed CO_2 due to aerosols. *Atmos. Chem. Phys.* **2005**, *5*, 3003–3013, doi:10.5194/acp-5-3003-2005.
3. Guerlet, S.; Butz, A.; Schepers, D.; Basu, S.; Hasekamp, O.P.; Kuze, A.; Yokota, T.; Blavier, J.F.; Deutscher, N.M.; Griffit, D.W.T.; et al. Impact of aerosol and thin cirrus on retrieving and validating XCO_2 from GOSAT shortwave infrared measurements. *J. Geophys. Res. Atmos.* **2013**, *118*, 4887–4905, doi:10.1002/jgrd.50332.
4. Barkley, M.P.; Frieß; U.; Monks, P.S. Measuring atmospheric CO_2 from space using Full Spectral Initiation (FSI) WFM-DOAS. *Atmos. Chem. Phys.* **2006**, *6*, 3517–3534, doi:10.5194/acp-6-3517-2006.

5. Miller, C.E.; Crisp, D.; DeCola, P.L.; Olsen, S.C.; Randerson, J.T.; Michalak, A.M.; Alkhaled, A.; Rayner, P.; Jacob, D.J.; Suntharalingam, P.; et al. Precision requirements for space-based X_{CO2} data. *J. Geophys. Res.* **2007**, *112*, D10314, doi:10.1029/2006JD007659.
6. Schneising, O.; Buchwitz, M.; Burrows, J.P.; Bovensmann, H.; Reuter, M.; Notholt, J.; Macatangay, R.; Warneke, T. Three years of greenhouse gas column-averaged dry air mole fractions retrieved from satellite–Part 1: Carbon dioxide. *Atmos. Chem. Phys.* **2008**, *8*, 3827–3853. https://doi.org/10.5194/acp-8-3827-2008.
7. Bösch, H.; Toon, G.C.; Sen, B.; Washenfelder, R.A.; Wennberg, P.O.; Buchwitz, M.; De Beek, R.; Burrows, J.P.; Crisp, D.; Christi, M.; et al. Space-based near-infrared CO_2 measurements: Testing the Orbiting Carbon Observatory retrieval algorithm and validation concept using SCIAMACHY observations over Park Falls, Wisconsin. *J. Geophys. Res.* **2006**, *111*, D23302, doi:10.1029/2006JD007080.
8. Yokota, T.; Yoshida, Y.; Eguchi, N.; Ota, Y.; Tanaka, T.; Watanabe, H.; Maksyutov, S. Global Concentrations of CO_2 and CH_4 Retrieved from GOSAT: First Preliminary Results. *Sola* **2009**, *5*, 160–163, doi:10.2151/sola.2009-041.
9. Crisp, D.; Fisher, B.M.; O'Dell, C.; Frankenberg, C.; Basilio, R.; Bösch, H.; Brown, L.R.; Castano, R.; Connor, B.; Deutscher, N.M.; et al. The ACOS XCO_2 retrieval algorithm, Part 2: Global XCO_2 data characterization. *Atmos. Meas. Tech.* **2012**, *5*, 687–707, doi:10.5194/amt-5-687-2012.
10. Yue, T.X.; Zhang, L.L.; Zhao, M.W.; Wang, Y.F.; Wilson, J.P. Space- and ground-based CO_2 measurements: A review. *Sci. China Earth Sci.* **2016**, *59*, 2089–2097, doi:10.1007/s11430-015-0239-7.
11. Chen, L.F.; Zhang, Y.; Zou, M.M.; Xu, Q.; Li, L.J.; Li, X.Y.; Tao, J.H. Overview of atmospheric CO_2 sensing from space. *J. Remote Sens.* **2015**, *19*, 1–11, doi:10.11834/jrs.20153331.
12. Chen, X.; Liu, Y.; Cai, Z.N. Review of Radiative Transfer Model in Retrieval of Atmospheric CO_2 from Satellite Shortwave Infrared Measurements. *Remote Sens. Technol. Appl.* **2015**, *30*, 825–834, doi:10.11873/j.issn.1004-0323.2015.5.0825.
13. Zhang, X.Y.; Zhou, M.Q.; Wang, W.H.; Li, X.J. Progress of global satellite remote sensing of atmospheric compositions and its' applications. *Sci. Technol. Rev.* **2015**, *33*, 13–22, doi:10.3981/j.issn.1000-7857.2015.17.001.
14. Chen, X.; Liu, Y.; Yang, D.X.; Cai, Z.N.; Chen, H.B.; Wang, M.H. A Theoretical Analysis for Improving Aerosol-Induced CO_2 Retrieval Uncertainties Over Land Based on TanSat Nadir Observations Under Clear Sky Conditions. *Remote Sens.* **2019**, *11*, 1061, doi:10.3390/rs11091061.
15. Oshchepkov, S.; Bril, A.; Yokota, T. PPDF-based method to account for atmospheric light scattering in observations of carbon dioxide from space. *J. Geophys. Res.* **2008**, *113*, D23210, doi:10.1029/2008JD010061.
16. Boesch, H.; Baker, D.; Connor, B.; Crisp, D.; Miller, C. Global Characterization of CO_2 Column Retrievals from Shortwave-Infrared Satellite Observations of the Orbiting Carbon Observatory-2 Mission. *Remote Sens.* **2011**, *3*, 270–304, doi:10.3390/rs3020270.
17. Yoshida, Y.; Ota, Y.; Eguchi, N.; Kikuchi, N.; Nobuta, K.; Tran, H.; Morino, I.; Yokota, T. Retrieval algorithm for CO_2 and CH_4 column abundances from short-wavelength infrared spectral observations by the Greenhouse gases observing satellite. *Atmos. Meas. Tech.* **2011**, *4*, 717–734, doi:10.5194/amt-4-717-2011.
18. O'dell, C.W.; Connor, B.; Boesch, H.; O'brien, D.; Frankenberg, C.; Castano, R.; Christi, M.; Crisp, D.; Eldering, A.; Fisher, B.; et al. The ACOS CO_2 retrieval algorithm-Part 1: Description and validation against synthetic observations. *Atmos. Meas. Tech.* **2012**, *5*, 99–121, doi:10.5194/amt-5-99-2012.
19. Liu, Y.; Yang, D.X.; Cai, Z.N. A retrieval algorithm for TanSat XCO_2 observation: Retrieval experiments using GOSAT data. *Chin. Sci. Bull.* **2013**, *58*, 1520–1523, doi:10.1007/s11434-013-0568-y.
20. Heymann, J.; Reuter, M.; Hilker, M.; Buchwitz, M.; Schneising, O.; Bovensmann, H.; Burrows, J.P.; Kuze, A.; Suto, H.; Deutscher, N.M.; et al. Consistent satellite XCO_2 retrievals from SCIAMACHY and GOSAT using the BESD algorithm. *Atmos. Meas. Tech.* **2015**, *8*, 2961–2980, doi:10.5194/amt-8-2961-2015.
21. Zhou, M.Q.; Zhang, X.Y.; Wang, P.C.; Wang, S.P.; Guo, L.L.; Hu, L.Q. XCO_2 satellite retrieval experiments in short-wave infrared spectrum and ground-based validation. *Sci. China Earth Sci.* **2015**, *58*, 1191–1197, doi:10.1007/s11430-015-5080-z.
22. Zhang, X.Y.; Zhang, P.; Liao, H.; Hu, X.Q.; Li, Y.; Zhang, L.J.; Rong, Z.G.; Qiu, H. On Ground-based Remote Sensing for Atmospheric Species by FTIR Instrument and Retrieval Algorithm. *Meteorol. Mon.* **2009**, *35*, 9–17.
23. Buchwitz, M.; Khlystova, I.; Bovensmann, H.; Burrows, J.P. Sciamachy/Wfm-Doas Tropospheric CO, CH_4, and CO_2 Scientific Data Products: Validation and Recent Developments. *Eur. Space Agency ESA* **2007**, SP-642.

24. Reuter, M.; Bovensmann, H.; Buchwitz, M.; Burrows, J.P.; Connor, B.J.; Deutscher, N.M.; Griffith, D.W.T.; Heymann, J.; Keppel-Aleks, G.; Messerschmidt, J.; et al. Retrieval of atmospheric CO_2 with enhanced accuracy and precision from SCIAMACHY: Validation with FTS measurements and comparison with model results. *J. Geophys. Res*. **2011**, *116*, D04301, doi:10.1029/2010JD015047.
25. Oshchepkov, S.; Bril, A.; Yokota, T.; Morino, I.; Yoshida, Y.; Matsunaga, T.; Belikov, D.; Wunch, D.; Wennberg, P.; Toon, G.; et al. Effects of atmospheric light scattering on spectroscopic observations of greenhouse gases from space: Validation of PPDF-based CO_2 retrievals from GOSAT. *J. Geophys. Res.* **2012**, *117*, D12305, doi:10.1029/2012JD017505.
26. Yoshida, Y.; Kikuchi, N.; Morino, I.; Uchino, O.; Oshchepkov, S.; Bril, A.; Saeki, T.; Schutgens, N.; Toon, G.C.; Wunch, D.; et al. Improvement of the retrieval algorithm for GOSAT SWIR XCO_2 and XCH_4 and their validation using TCCON data. *Atmos. Meas. Tech.* **2013**, *6*, 1533–1547, doi:10.5194/amt-6-1533-2013.
27. Wunch, D.; Wennberg, P.O.; Osterman, G.; Fisher, B.; Naylor, B.; Roehl, C.M.; O'dell, C.; Mandrake, L.; Viatte, C.; Kiel, M.; et al. Comparisons of the Orbiting Carbon Observatory-2 (OCO-2) XCO_2 measurements with TCCON. *Atmos. Meas. Tech.* **2017**, *10*, 2209–2238, doi:10.5194/amt-10-2209-2017.
28. Bi, Y.M.; Wang, Q.; Yang, Z.D.; Chen, J.; Bai, W.G. Validation of column-averaged dry-air mole fraction of CO_2 retrieved from $OCO\text{-}_2$ using ground-based FTS measurements. *J. Meteor. Res.* **2018**, *32*, 433–443, doi:10.1007/s13351-018-7118-6.
29. Liu, Y.; Wang, J.; Yao, L.; Chen, X.; Cai, Z.N.; Yang, D.X.; Yin, Z.S.; Gu, S.Y.; Tian, L.F.; Lu, N.M.; et al. The TanSat mission: Preliminary global observations. *Sci. Bull.* **2018**, *63*, 1200–1207, doi:10.1016/j.scib.2018.08.004.
30. Wunch, D.; Toon, G.C.; Blavier, J.-F.L.; Washenfelder, R.A.; Notholt, J.; Connor, B.J.; Griffith, D.W.T.; Sherlock, V.; Wennberg, P.O. The Total Carbon Column Observing Network. *Philos. Trans. Roy. Soc. A* **2011**, *369*, 2087–2112, doi:10.1098/rsta.2010.0240.
31. Zhang, X.Y.; Meng, X.Y.; Zhou, M.Q.; Bai, W.G.; Zhou, L.H.; Hu, Y.M.; Yu, X. Review of the validation of atmospheric CO_2 from satellite hyper spectral remote sensing. *Clim. Chang. Res.* **2019**, *14*, 602–612, doi:10.12006/j.issn.1673-1719.2018.070.
32. Rozanov, V.V.; Dinter, T.; Rozanov, A.V.; Wolanin, A.; Bracher, A.; Burrows, J.P. Radiative transfer modeling through terrestrial atmosphere and ocean accounting for inelastic processes: Software package SCIATRAN. *J. Quant. Spectrosc. Radiat. Transf.* **2017**, *194*, 65–85, doi:10.1016/j.jqsrt.2017.03.009.
33. Rodgers, C.D. *Inverse Methods for Atmospheric Sounding: Theory and Practice*; World Scientific: Singapore, 2000.
34. Liu, D.D.; Zhang, C.M.; Li, Y.F.; Zhang, X.Y.; Wang, S.P.; Zhang, L.; Zhang, P.; Chen, J.; Rong, P. The retrieval algorithm for a satellite-borne CO_2-sounder: Preliminary results in near infrared band. *Optik* **2016**, *127*, 8613–8620, doi:10.1016/j.ijleo.2016.06.072.
35. Wang, D.Y.; Liu, D.D. Preliminary results of X_{CO2} retrieval from hyperspectral observations of TanSat. *Ecol. Environ. Monit. Three Gorges* **2018**, *3*, 74–81, doi:10.19478/j.cnki.2096-2347.2018.04.12.
36. Marquardt, D.W. An algorithm for least squares estimation of nonlinear parameters. *J. Soc. Ind. Appl. Math.* **1963**, *11*, 431–441.
37. Lin, C.; Li, C.L.; Wang, L.; Bi, Y.M.; Zheng, Y.Q. Preflight spectral calibration of hyperspectral carbon dioxide spectrometer of TanSat. *Opt. Precis. Eng.* **2017**, *25*, 2064–2075, doi:10.3788/OPE.20173508.2064.
38. Zhang, H.; Zheng, Y.Q.; Lin, C.; Wang, W.Q.; Wang, Q.; Li, L. Laboratory spectral calibration of TanSat and the influence of multiplex merging of pixels. *Int. J. Remote Sens.* **2017**, *38*, 3800–3816, doi:10.1080/01431161.2017.1306142.
39. Zhang, L.L.; Yue, T.X.; Wilson, J.P.; Wang, D.Y.; Zhao, N.; Liu, Y.; Liu, D.D.; Du, Z.P.; Wang, Y.F.; Lin, C.; et al. Modelling of XCO_2 Surfaces Based on Flight Tests of TanSat Instruments. *Sensors* **2016**, *16*, 1818, doi:10.3390/s16111818.
40. Wunch, D.; Wennberg, P.O.; Toon, G.C.; Connor, B.J.; Fisher, B.; Osterman, G.B.; Frankenberg, C.; Mandrake, L.; O'dell, C.; Ahonen, P.; et al. A method for evaluating bias in global measurements of CO_2 total columns from space. *Atmos. Chem. Phys.* **2011**, *11*, 12317–12337.

41. O'dell, C.W.; Eldering, A.; Wennberg, P.O.; Crisp, D.; Gunson, M.R.; Fisher, B.; Frankenberg, C.; Kiel, M.; Lindqvist, H.; Mandrake, L.; et al. Improved retrievals of carbon dioxide from Orbiting Carbon Observatory-2 with the version 8 ACOS algorithm. *Atmos. Meas. Tech.* **2018**, *11*, 6539–6576, doi:10.5194/amt-11-6539-2018.
42. Cogan, A.J.; Boesch, H.; Parker, R.J.; Feng, L.; Palmer, P.I.; Blavier, J.F.L.; Deutscher, N.M.; Macatangay, R.; Notholt, J.; Roehl, C.; et al. Atmospheric carbon dioxide retrieved from the Greenhouse gases Observing SATellite (GOSAT): Comparison with ground-based TCCON observations and GEOS-Chem model calculations. *J. Geophys. Res. Atmos.* **2012**, *117*, D21301, doi:10.1029/2012JD018087.